Associative detachment, dissociative attachment and vibrational excitation of HCl by low-energy electrons

M. Čížek*, J. Horáček

Department of Theoretical Physics, Faculty of Mathematics and Physics,
Charles University Prague, V Holešovičkách 2, 180 00 Praha 8, Czech Republic

W. Domcke

Institute of Theoretical Chemistry, Heinrich Heine University,
Universitätstrasse 1, D-40225 Düsseldorf

(April 13, 2001)

Abstract

An improved nonlocal resonance model for electron-HCl collisions is constructed. The model takes account of the dependence of the dipole-modified threshold exponent on the internuclear distance. The long-range part of the HCl$^-$ potential-energy function has been determined from the most accurate ab initio calculations which are available. Only the s-wave component of the electronic continuum wave function is taken into account. Cross sections for vibrational excitation, dissociative attachment and associative detachment have been calculated. For all three collision processes, the cross sections calculated with the new model are in better agreement with experiment than previous calculations. The calculations reproduce very well even fine details of the threshold structures in the vibrational excitation cross sections of HCl.
(suggested) PACS numbers: 34.50.-s,34.80.Ht,34.80.-i

Typeset using REVTEX

I. INTRODUCTION

The collision of low-energy electrons with the HCl molecule represents a typical example of a molecular resonance process in which the polar nature of the molecular target plays an important role. The resonant character of the collision leads to large cross sections for inelastic and reactive processes, i.e., vibrational excitation (VE), dissociative electron attachment(DA) and the inverse process of associative detachment (AD). These processes have been studied by various authors both experimentally and theoretically.

The most interesting feature in hydrogen halides is the existence of pronounced threshold peaks in the VE cross sections observed first by Rohr and Linder [1,2]. The cross sections in the threshold region attain very high values and represent the highest vibrationally inelastic cross sections measured. The step-like structures in the DA cross section (Wigner cusps) first observed by Abouaf and Teillet-Billy [3] represent another striking feature of low-energy electron-HCl collisions. More recently, additional fine structure has been discovered in the $0 \rightarrow 1$ and $0 \rightarrow 2$ VE functions of HCl, which appears in the form of oscillations converging towards the DA threshold [4,5].

Several theoretical models have been put forward to provide an explanation of these unusual phenomena [6–15]. They are based on a variety of theoretical concepts such as the projection-operator formalism [6,7,10,11,15], the R-matrix formalism [12–14], or the zero-range potential model [8,9]. The so-called nonlocal resonance model developed by Domcke and Mündel [11] has so far provided the most complete description of the resonance and threshold features observed in low-energy electron-HCl collisions [4,16,17]. This model describes qualitatively all the observed features: threshold peaks and broad resonances in the VE cross sections, Wigner cusps in the DA cross sections, as well as oscillatory structures in the VE cross sections below the threshold of the DA channel. This type of model has also been used by Horáček et al. for the calculation of VE and DA cross sections in HBr [18] and HI [19].

As applied to the HCl molecule, the model of Domcke and Mündel (henceforth referred to as DM) has certain shortcomings. The main parameter determining the cross sections at very low energies is the threshold exponent α. This parameter is, in the case of polar molecules, determined by the dipole moment, which in turn depends on the internuclear distance. This means that the threshold exponent α also depends on the internuclear distance. In all previous applications of this model it was assumed that the threshold exponent is a constant equal to the value of α taken at the equilibrium internuclear distance. This approximation greatly simplifies the calculations, but its validity and accuracy has not been tested. In a recent paper by Horáček et al. [20], it was shown that the approximation of constant α is a very good approximation for HBr and HI molecules which possess weak dipole moments, but is not adequate for the calculation of VE cross sections of HCl.

In the present work we elaborate a further improvement of the DM model which is necessary for the calculation of the AD cross section. While the overall magnitude of the VE and DA cross sections is not sensitive to the H-Cl$^-$ potential-energy function at large internuclear distances, the magnitude of the AD cross section is largely determined by this part of the HCl$^-$ potential. In the DM model the nonlocal potential-energy function at short and intermediate internuclear distances has been determined by fitting ab initio electron-HCl scattering data of Padial and Norcross [22]; the long-range part of the potential has been constructed by extrapolation [11]. In the meantime accurate ab initio calculations of the long-range part of the HCl$^-$ $^2\Sigma^+$ potential-energy function have been reported by O'Neil at al. [23] and Åstrand and Karlström [24]. In the present work we make use of these data to construct an improved nonlocal resonance model for HCl which is suitable for the calculation of the AD cross section. It will be shown that this improvement of the DM model, together with the variable threshold exponent introduced by Horáček et al. [20], also leads to a significant improvement of the calculated VE and DA cross sections.

A calculation of the AD cross section in low-energy H + Cl$^-$ collisions based on a zero-range-potential model has been reported by Gauyacq [25]. The present work represents the first treatment of the H + Cl$^-$ AD process in the nonlocal complex-potential formalism. This calculation is computationally considerably more demanding than calculations for the inverse process of DA. While only few partial waves are involved in the DA process, many partial waves have to be taken into account to obtain a converged cross section for the AD process. It should also be stressed that the local-complex- potential approximation is inapplicable for low-energy H + Cl^- collisions owing to the threshold singularities caused by the dipole potential in the electron-scattering channel [17]. In contrast to the H + H^- collision, where the local-complex-potential approximation is of quantitative accuracy for the AD process [26], a nonlocal treatment is indispensable for the H+ Cl^- AD process.

II. NONLOCAL RESONANCE FORMALISM

Since the nonlocal resonance model has been described in reviews [16,17] we give here only a brief description of the essentials needed to comprehend the paper.

In the nonlocal resonance model it is assumed that a quasi-stationary molecular negative-ion state is formed during the collision process. This resonance state is represented by its discrete component $|\varphi_d\rangle$ which is assumed to interact with a continuum of states $|\varphi_\epsilon\rangle$ orthogonal to $|\varphi_d\rangle$, describing electrons with energy ϵ scattered by the neutral molecule in its ground electronic state. The Hamiltonian H of such a resonance model including nuclear motion can be written as $H = T_\mathrm{N} + H_\mathrm{el}$, where [17]

$$\begin{aligned} H_\mathrm{el} = |\varphi_d\rangle V_d(R) \langle\varphi_d| + \int d\epsilon d\Omega |\varphi_\epsilon\rangle [V_0(R) + \epsilon] \langle\varphi_\epsilon| + \\ + \int d\epsilon d\Omega |\varphi_d\rangle V_{d\epsilon}(R) \langle\varphi_\epsilon| + \int d\epsilon d\Omega |\varphi_\epsilon\rangle V^*_{d\epsilon} \langle\varphi_d|, \end{aligned} \tag{1}$$

R is the internuclear distance, T_N denotes the kinetic-energy operator of the nuclei, V_0 is the adiabatic potential energy for the ground electronic state of HCl, V_d is the discrete-state potential, and $V_{d\epsilon}$ the discrete-state-continuum coupling. The functions $V_d(R)$, $V_0(R)$ and $V_{d\epsilon}(R)$ determine the model.

The special form (1) of the Hamiltonian, i.e., the explicit appearance of the discrete state $|\varphi_d\rangle$ and the orthogonal states $|\varphi_\epsilon\rangle$, makes it possible to reduce the full Schrödinger equation by projecting onto a subspace defined by the discrete-state wave function,

$$(T_N + V_d - E)|\Psi_d\rangle = \\ -\int d\epsilon d\Omega V_{d\epsilon}(E - \epsilon - T_{\rm N} - V_0 + i\varepsilon)^{-1} V^*_{d\epsilon}|\Psi_d\rangle, \qquad (2)$$

where $|\Psi_d\rangle$ is the projection of the complete wave function on $|\varphi_d\rangle$. Here $|\Psi_d\rangle$ is still a ket vector in the Hilbert space of nuclear motion; ε is the usual positive infinitesimal.

Making use of the partial wave expansion of $|\Psi_d\rangle$ and of the Green's function, we obtain the basic dynamical equation of the nonlocal resonance model [26,27]

$$|\psi_l\rangle = |\phi_l\rangle + G_l(E)[V_d + F_l(E)]|\psi_l\rangle, \qquad (3)$$

where

$$\langle R|F_l(E)|R'\rangle = \int d\epsilon d\Omega V_{d\epsilon}(R) g_l(E - \epsilon, R, R') V^*_{d\epsilon}(R') \qquad (4)$$

and

$$g_l(E) = \left(E + \frac{1}{2\mu}\frac{d^2}{dR^2} - V_0(R) - \frac{l(l+1)}{2\mu R^2} + i\varepsilon\right)^{-1}. \qquad (5)$$

The function $|\phi_l\rangle$ denotes the partial wave function of free nuclear motion with the energy $E = K^2/2\mu$

$$\langle R|\phi_l\rangle = R j_l(KR), \qquad (6)$$

$|\psi_l\rangle$ is the partial wave contribution to $|\Psi_d\rangle$ corresponding to the angular momentum l, and $G_l(E)$ is the l-component of the free Green's function.

Following Bieniek [27], the formula for the total AD cross section is

$$\sigma_{\rm AD} = \frac{4\pi^2}{E}\sum_{l=0}^{\infty}(2l+1)\sum_{\nu}|\langle\psi_l|V_{d\epsilon_{\rm f}}|\chi_l^\nu\rangle|^2. \qquad (7)$$

Here the kets $|\chi_l^\nu\rangle$ denote bound-state wave functions of HCl (ν is the vibrational quantum number). The energy $\epsilon_{\rm f}$ in (7) refers to the outgoing electron and is given by the energy-conservation law $\epsilon_{\rm f} = E - E_l^\nu$, where E_l^ν is the energy of the bound state $|\chi_l^\nu\rangle$.

The cross section for dissociative attachment of an electron to a molecule in the state $|\chi_l^\nu\rangle$ is given by the formula [17]

$$\sigma_{\mathrm{DA}} = \frac{4\pi^2\mu}{\epsilon_{\mathrm{i}}} |\langle\psi_l|V_{d\epsilon_{\mathrm{i}}}|\chi_l^{\nu}\rangle|^2. \tag{8}$$

The energy ϵ_{i} refers to the incoming electron and the energy conservation determines the kinetic energy E of the outgoing nuclei.

Finally, the cross section for vibrational excitation can be calculated as [17]

$$\begin{aligned}\sigma_{\mathrm{VE}} &= \frac{2\pi^3}{\epsilon_{\mathrm{i}}} |\langle\chi_l^{\nu_{\mathrm{f}}}|V_{d\epsilon_{\mathrm{f}}}^{*}\left(E + \frac{1}{2\mu}\frac{d^2}{dR^2} - V_d - F_l(E) - \frac{l(l+1)}{2\mu R^2} + i\varepsilon\right)^{-1} V_{d\epsilon_{\mathrm{i}}}|\chi_l^{\nu_{\mathrm{i}}}\rangle|^2 \\ &= \frac{2\pi^3}{\epsilon_{\mathrm{i}}} |\langle\chi_l^{\nu_{\mathrm{f}}}|V_{d\epsilon_{\mathrm{f}}}^{*}|\psi_l^{\nu_{\mathrm{i}}}\rangle|^2, \end{aligned} \tag{9}$$

where $|\psi_l^{\nu_{\mathrm{i}}}\rangle$ is the solution of the equation (3), but now with

$$|\phi_l\rangle = G_l(E) V_{d\epsilon_{\mathrm{i}}}|\chi_l^{\nu_{\mathrm{i}}}\rangle. \tag{10}$$

Energy conservation gives $\epsilon_{\mathrm{i}} + E_l^{\nu_{\mathrm{i}}} = E = \epsilon_{\mathrm{f}} + E_l^{\nu_{\mathrm{f}}}$. No rotational excitation is possible if $V_{d\epsilon}$ is of pure s-wave character.

III. GENERALIZATION OF THE MODEL

The nonlocal resonance model is given in terms of the functions $V_d(R)$, $V_0(R)$ and $V_{d\epsilon}(R)$ describing the discrete state of the negative ion, the neutral ground state and the discrete-state-continuum coupling. In the DM model these functions are represented as follows

$$V_d(R) = D_1 \mathrm{e}^{-\alpha_1(R-R_0)}\left(\mathrm{e}^{-\alpha_1(R-R_0)} - 2t\right), \tag{11}$$

$$V_0(R) = D_0 \mathrm{e}^{-\alpha_0(R-R_0)}\left(\mathrm{e}^{-\alpha_0(R-R_0)} - 2\right) + Q_0, \tag{12}$$

$$V_{d\epsilon}(R) = a\left(\frac{\epsilon}{b}\right)^{\alpha/2} \mathrm{e}^{-\epsilon/2b} g(R). \tag{13}$$

$$g(R) = \begin{cases} \exp(-CR) & , R \le R_1 \\ \exp(-CR - D(R-R_1)) & , R > R_1 \end{cases} \tag{14}$$

The values of the parameters for HCl are given in [11].

The dependence of the threshold exponent on the internuclear distance has recently been introduced by Horáček et al. [20]. This modified DM model will henceforth be referred to as

DMH model. The threshold exponent α in Eq. (13) is replaced by a general function $\alpha(R)$, i.e.,

$$V_{d\epsilon}(R) = a \left(\frac{\epsilon}{b}\right)^{\alpha(R)/2} \mathrm{e}^{-\epsilon/2b} g(R). \tag{15}$$

Note that the coupling $V_{d\epsilon}(R)$ is no longer a separable function of the variables ϵ and R, as it was in the DM model. The threshold exponent $\alpha(R)$ has been determined from the ab initio calculated dipole moment function of HCl [21].

A further improvement of the model is achieved by a better description of the long-range part of the negative-ion potential function. The constants α_1, D_1, t in $V_d(R)$, the function $g(R)$ and the constants a, b in $V_{d\epsilon}(R)$ were obtained by Domcke and Mündel by fitting fixed-R ab initio electron-HCl scattering data for R ranging from 1.8 to 3 a.u. No information on the potential-energy function at larger internuclear distances has been used in this model. Several accurate ab initio studies of the bound part of the ${}^2\Sigma^+$ potential of HCl$^-$ are now available in the literature [23,24]. This makes it possible to further improve the DM model.

To do so we define the potential $V_1(R)$ of the ${}^2\Sigma^+$ resonance and bound state of HCl$^-$ as

$$V_1(R) = V_0(R) + E_{\mathrm{Res}}(R), \tag{16}$$

where

$$E_{\mathrm{Res}}(R) = V_d(R) - V_0(R) + \Delta(E_{\mathrm{Res}}(R), R). \tag{17}$$

The level shift $\Delta(E, R)$ is defined as

$$\Delta(E, R) = \tfrac{1}{2\pi} \mathrm{P} \int_0^\infty \frac{|V_{d\epsilon}(R)|^2}{E - \epsilon} d\epsilon. \tag{18}$$

If $E_{\mathrm{Res}} < 0$, then $V_1(R)$ represents the bound electronic state of HCl$^-$. This holds for $R > 2.8$ a.u. If $E_{\mathrm{Res}} > 0$, then $V_1(R)$ represents the ${}^2\Sigma^+$ shape resonance. The the discrete-state potential $V_d(R)$ can now be expressed in terms of $V_1(R)$, $V_0(R)$ and $\Delta(E, R)$

$$V_d(R) = V_1(R) - \Delta(V_1(R) - V_0(R), R). \tag{19}$$

An improved model exhibiting the correct long-range behaviour of the HCl^- potential function can thus be constructed by modifying the function $V_d(R)$ while retaining the functions $V_0(R)$ and $V_{d\epsilon}(R)$ (equations (12) and (15)). For this we used the ab initio data of O'Neil et al. [23] and of Åstrand and Karlström [24]. A spline interpolation has been used to obtain $V_d(R)$ and the potential was smoothly matched to the polarization potential $-2.25\text{a.u.}/\text{R}^4$ at large R. The original form (11) of $V_d(R)$ has been used for $R < 2.8$ a.u. where it has been determined from ab initio fixed-R electron-molecule scattering data [11].

Finally, for computational convenience, we have replaced the spline interpolation of $V_d(R)$ by a simple analytic formula. To remove the kink in the function $g(R)$ of Eq.(14) at $R = R_1$, we modified the function $g(R)$ to render it a smooth function of R at $R = R_1$. For a detailed description of these technical aspects we refer to the Appendix.

In the following the models resulting from the long-range ab initio data of O'Neil et al. and Åstrand and Karlström will be referred to as DMHC-1 and DMHC-2 models, respectively. The potential function $V_0(R)$ and the functions $V_1(R)$ of the DM, DMHC-1 and DMHC-2 models are shown in figure 1 together with the ab initio data.

The DMHC-2 model is considered as the definitive model, since the Åstrand and Karlström data are judged to be more accurate than the O'Neil data. In the following we report also results for the DM, DMH and DMHC-1 models, to indicate the sensitivity of the cross sections to details of the model.

IV. CALCULATION OF CROSS SECTIONS

The cross sections are obtained from Eqs.(7), (8) and (9), where the wave function $|\psi_l\rangle$ is the unique solution of the effective Lippmann-Schwinger equation (3). To solve this equation we employ the Schwinger-Lanczos method, which proved to be very efficient for the calculation of VE and DA cross sections for HBr, HCl, HI and H_2 molecules [18,19,26]. For a detailed description of the Schwinger-Lanczos method, see [28]. For the treatment of the nonseparable coupling matrix element $V_{d\epsilon}(R)$ due to the variable threshold exponent $\alpha(R)$

we use the Batemann technique described in [20].

Convergence of the partial-wave sum for the AD cross section for a collision energy of 1eV requires the inclusion of angular momenta up to $l_{max} = 38$.

V. RESULTS

A. Associative detachment

We consider first the AD cross section, since this is a highly integrated quantity providing little insight into the details of the dynamics. A calculation of the AD cross section in low-energy H + Cl^- collisions based on a zero-range-potential model has been performed by Gauyacq [25]. The parameters of the model were adjusted to reproduce the available experimental data [25]. Here we perform this calculation with an ab-initio-based model which contains no parameters which are adjusted to experimental data (except spectroscopic data of the neutral ground state of HCl, which are also available from accurate ab initio calculations [29]). It should be stressed, moreover, that we employ one and the same model to calculate cross sections for all channels (VE, DA and AD).

The total AD cross sections obtained with the DM, DMHC-1 and DMHC-2 models are shown in figure 2 together with the experimental data [30]. At collision energies above 1 eV all three models yield the same cross section. At low energies (below 100 meV) only the DMHC-2 model yields a AD cross section which is consistent with the cross section inferred from rate coefficients of Fehsenfeld et al. [31]. The significant deviation of the DMHC-1 cross section from the DMHC-2 cross section and experiment at low energies reflects the fact that the potential of O'Neil et al. is not sufficiently attractive at large and intermediate distances (cf. Fig. 1). It can be concluded that only the Åstrand and Karlström HCl^- potential-energy function is compatible with the measured low-energy H + Cl^- AD cross section.

The AD cross section exhibits an extended series of threshold peaks, each at the opening of a rovibrational channel of the HCl molecule. Detailed plots of the threshold peaks in the AD cross section obtained with the DMHC-2 model are shown in Fig. 3. For higher E only the thresholds with $\nu = 0$ and $l \sim 50$ are discernible. For $E < 1.3$eV, the structure becomes more complicated because of the appearance of thresholds with $\nu > 0$.

B. Dissociative attachment

Calculations of the DA cross section for HCl have been reported by several authors, see, e.g. [6,9,11–15]. The majority of the calculations provides a qualitatively correct description of the observed features, i.e., an essentially vertical onset at threshold, step-like Wigner cusps at the openings of the VE channels, and a rapid increase of the cross section with increasing rovibrational energy of the target. It has been noted that the DA cross section for $\nu = 0, l = 0$ is generally less sensitive to details of the potential-energy functions than the VE cross sections [11,12,15]. The existing calculations taking full account of the nonlocality of the problem have been performed without inclusion of the rotational degrees of freedom ($l = 0$) [11,14,15,32].

Since in the real experiments the target gas is at nonzero temperature T, the target molecules may be excited either rotationally or vibrationally. To describe this situation we have calculated in the present work the DA cross section for target molecules in their four lowest vibrational states and for angular momenta $l = 0, \ldots, 30$ and then averaged the results over the Maxwell-Boltzmann distribution of the target states. The cross sections for the temperature T=1000 K is shown in figure 4 together with the experimental data of Allan and Wong [33]. To compare our results with the experimental data we convoluted the theoretical data with a Gaussian distribution with the full width at half maximum (FWHM) equal to the energy spread of the electrons in the experiment (50meV). Moreover, since Allan and Wong give the uncertainty of their energy scale as ± 40meV, we have also shifted the experimental data to higher energies by 35meV. In this way the positions of the calculated cross section peaks agree perfectly with the measured data.

Let us first discuss the theoretical results for the different models. The influence of the long-range part of the potential is seen in the difference among the DM, DMHC-1 and DMHC-2 models. The more attractive the interaction, the larger the cross section for DA at low-collision energies. The cross section exhibits two dominant features: peaks for electron energy below 1eV and step-like structures above this energy. The steps known as Wigner cusps are related to the opening of the $0 \to 3$ and $0 \to 4$ vibrational excitation channels. The highest peak originates from molecules in their ground vibrational state ($\nu = 0$) and small angular momentum l; it is situated close to the threshold for dissociative attachment to molecules in the ground state. The second peak is due to HCl molecules in $\nu = 0$ and $l \sim 15$ states and it appears just below the threshold for $0 \to 2$ vibrational excitation. Its origin is clearly understood if we look at figure 5, where the cross sections for attachment to HCl molecules with $\nu = 0$ and several l are shown (DMHC-2 model). The cross sections for $l > 10$ exhibit high peaks near the threshold which are suppressed in the thermal average by the Maxwell-Boltzmann factor $(2l+1)\exp(-(E_l^\nu - E_0^0)/kT)$, which is decreasing with l for $l > 10$. It is also clear from figure 5 that the peak is related to the Wigner cusp at the $0 \to 2$ VE threshold. Contributions from HCl molecules in the $\nu = 1$ state are also seen in the cross section as a shoulder at the $(\nu = 1, l \sim 0)$ DA threshold and as a peak below the $1 \to 2$ VE threshold in figure 4.

Comparing the theoretical data with the experiment of Allan and Wong, we see that the position of the structures agrees quite well (accepting the shift, see above) but their relative height differs significantly. It is worth to point out that perfect agreement between theory and the measured data may be obtained by assuming a higher temperature of the target gas. This is demonstrated in figure 6. If, for example, the cross section calculated at the temperature T=1230 K is compared with the data measured at T=1000 K we observe perfect agreement. The same holds also for other temperatures as indicated in figure 6. Since perfect agreement between theory and experiment can be obtained in all cases (see Fig. 6), we conjecture that a systematic error in the measurement of the temperature in the experiment of Allan and Wong may be responsible for the discrepancies between theory and experiment. The temperatures given by Allan and Wong appear to be systematically too low by 10-30%.

C. Vibrational excitation

Let us finally proceed to the discussion of the vibrational excitation process. Previous calculations [11,14,15] have described qualitatively the observed features, i.e., the threshold peaks and the broad resonance region, but the detailed shapes of the cross sections were not reproduced correctly. Here we demonstrate that for energies close to the threshold the modifications of the original DM model proposed in this paper improve the agreement between theory and experiment to such an extent that not only the gross features, but also very minute details of the calculated cross sections can be compared with the measured data.

It has been shown in [20] that taking the variation of α with R into account changes the cross section near threshold significantly for molecules with larger dipole moments (HCl), but has only a marginal effect for molecules with small dipole moments (HBr and HI). The agreement between theory and experiment is further improved when the long-range behaviour of the HCl^- potential function is corrected according to ab initio calculations. The effect of both modifications is shown in figures 7a–7d, where the $0 \rightarrow 1$ VE cross section for HCl is plotted. The cross section obtained with the DM model is shown in figure 7a; the cross section in figures 7b and 7c has been obtained with the DMHC-2 model, incorporating the R dependence of the threshold exponent and the long-range ab initio data of Åstrand and Karlström. For better comparison with experiment the data in figure 7b were convoluted with a Gaussian of 10 meV width and the data in figure 7c with a Gaussian of 20 meV width. Finally, in figure 7d, the experimental cross section of Schafer and Allan [5] is plotted. The same cross sections for the $0 \rightarrow 2$ transition are shown in figures 8a–8d. The results demonstrate the dramatic improvement in the shape and fine structure of the cross sections obtained by incorporation of the R-dependence of α and by correcting the long-range part of the HCl^- potential-energy function.

Let us now discuss in more detail the effect of the long-range part of the H + Cl^- interaction. Plots of non-convoluted $0 \to 1$ and $0 \to 2$ VE cross sections in the threshold region are shown in figure 9a and 9b. The effect of the long-range part of the interaction manifests itself most strongly for energies below the threshold of the DA channel. Both models, DMHC-1 and DMHC-2, predict oscillatory structures in an energy range which extends from the bottom of the respective potential curve $V_1(R)$ to the DA threshold. The oscillations reflect interference with quasi-bound levels supported by the attractive well at intermediate internuclear distances (cf. Fig. 1). Such oscillations have been predicted also by some other HCl models [15] and observed experimentally [4,5]. The DMHC-2 model constructed from the most sophisticated ab initio data predicts oscillations very similar to those seen in the high resolution experiments of Schafer and Allan [5] and Cvejanović [4] which are plotted in figure 10 together with convoluted DMHC-2 data. The positions of the calculated oscillations are somewhat shifted (10–20 meV) with respect to experiment, but the overall shape is in good agreement when the finite resolution and the contribution from several l (temperature 300K) in the experiment are taken into account.

The $0 \to \nu$ ($\nu = 0, 1, \ldots, 5$) cross sections[1] for electron energies up to 4eV are shown in figure 11 together with the (non-normalized) experimental data of Schafer and Allan [5]. Unlike the DA and AD data (at most 10% difference) the VE cross sections for energies above the DA threshold turn out to be strongly dependent on tiny differences of the models. The shape of the experimental cross sections is quite well reproduced and, except of $0 \to 1$ cross section, the difference between theory and experiment is within the uncertainty given by the difference between the DMHC-1 and DMHC-2 models.

---

[1] Cross sections for $\nu_1 \to \nu_2$, $\nu_1, \nu_2 = 0, 1, \ldots, 4$ transitions can be obtained on request from the authors.

VI. CONCLUSIONS

We have constructed an improved nonlocal resonance model for electron-HCl collisions and have performed calculations of VE, DA and AD cross sections. It can be summarized that the cross sections calculated with the new DMHC-2 model are in much better agreement with the experimental data for all processes considered here (AD, DA and VE) than any other calculation published so far. The generalization and improvement of the nonlocal resonance model proposed in this paper leads to almost perfect agreement between theory and experiment in the low-energy range. For VE at higher energies further improvements of the model may be required. New experiments would be valuable in which the dependence of DA cross section on the internal state of HCl is measured directly. These cross sections are closely related to the distribution of HCl states after associative detachment, which can be determined by measuring the energy spectrum of the released electrons.

Further improvements of the model within the scope of the resonance formalism are possible:

- We have seen that the VE cross sections are quite sensitive to the precise form of $V_{d\epsilon}(R)$. Direct ab initio calculation of $V_d(R)$ and $V_{d\epsilon}(R)$ would be useful.
- Recent measurements of the Kaiserslautern group [34–36] indicate that higher partial waves may contribute to e^-+HCl scattering. Our treatment ignores the angular momentum of the electron, which is equivalent to the assumption that only the s-wave contributes to $|\varphi_\epsilon\rangle$. It is not difficult to incorporate angular momentum transfer into our model (see [26]) but additional information about the partial-wave components of $V_{d\epsilon}(R)$ is necessary [37].

ACKNOWLEDGMENTS

This research was carried out in part during the stay of M. Č. at the Institute of Theoretical Chemistry of the Heinrich-Heine-University Düsseldorf. M. Č. would like to thank the staff of the institute for generous help and for the friendly environment. Support by the DAAD is gratefully acknowledged. M. Č. also acknowledges support from the Deutsche Forschungsgemeinschaft through Forschergruppe 'Niederenergetische Elektronenstreuprozesse' for a stay at Fachbereich Physik of the University of Kaiserslautern where part of his work was carried out.

APPENDIX: DESCRIPTION OF THE DMHC-2 MODEL

Atomic units are used unless stated otherwise.

For the potential of neutral HCl we assume the Morse function

$$V_0(R) = 0.169414e^{-1.002(R-R_0)}(\mathrm{e}^{-1.002(R-R_0)} - 2) + Q_0. \tag{A1}$$

derived from spectroscopic data [11]. The equilibrium distance is $R_0 = 2.409$ and the electron affinity of Cl is $Q_0 = 3.605\mathrm{eV} \doteq 0.132481$.

For the discrete-state potential we use the formula

$$\begin{aligned} V_d(R) = 0.086361\mathrm{e}^{-1.74628(R-R_0)} - \\ - \frac{2.25}{((R-3.5)^2 + 51.37)^2 - 2500} \end{aligned} \tag{A2}$$

which reasonably fits the $V_d(R)$ determined from ab initio data of Padial and Norcross (see section 3).

The discrete-state-continuum coupling is

$$V_{d\epsilon}(R) = g(R)f(\epsilon, R), \tag{A3}$$

where

$$g(R) = 1.07758(1 - 0.03101R)(1 + \mathrm{e}^{4.2(R-3.28)})^{-1} \tag{A4}$$

$$f(\epsilon, R) = 0.428785(\epsilon/b)^{\alpha(R)/2}\mathrm{e}^{-\epsilon/2b} \tag{A5}$$

and $b = 0.199732$. For $\alpha(R)$ we use an interpolation formula [21]

$$\alpha(R) = \tfrac{1}{2} + a_1 M^2 + a_2 M^4 + a_3 M^6 + a_4 M^8, \tag{A6}$$

with

$$M(R) = M_0 (1+R)^3 (1 + \textstyle\sum e_i R^i)^{-1}. \tag{A7}$$

The parameters a_i, e_i and M_0 are collected in the following table

$a_1 = -0.0101157$

$a_2 = -0.14833$

$a_3 = -0.07486$

$a_4 = -0.03735$

$M_0 = 1.09333$

$e_1 = 1.897$

$e_2 = 0.871$

$e_3 = 1.465$

$e_4 = 1.829$

$e_5 = -4.137$

$e_6 = 13.886$

$e_7 = 0.416.$

REFERENCES

* E-mail address: `cizek@mbox.troja.mff.cuni.cz`

[1] K. Rohr and F. Linder, J. Phys. B**8**, L200 (1975).

[2] K. Rohr and F. Linder, J. Phys. B**9**, 2521 (1976).

[3] R. Abouaf and D. Teillet-Billy, J. Phys. B**10**, 2261 (1977).

[4] S. Cvejanović, in: *18th Int. Conf. on Electronic and Atomic Collisions (ICPEAC)*, book of invited papers, Aarhus, (1993).

[5] O. Schafer and M. Allan, J. Phys. B**24**, 3069 (1991).

[6] F. Fiquet-Fayard, J. Phys. B**7**, 810 (1974).

[7] W. Domcke and L. S. Cederbaum, J. Phys. B**14**, 149 (1980).

[8] J. P. Gauyacq and A. Herzenberg, Phys. Rev. A**25**, 2959 (1982).

[9] D. Teillet-Billy and J. P. Gauyacq, J. Phys. B**17**, 4041 (1984).

[10] N. Bardsley and J. M. Wadehra, J. Chem. Phys. **78**, 7227 (1983).

[11] W. Domcke and C. Mündel, J. Phys. B**18**, 4491 (1985).

[12] I. I. Fabrikant, Z. Phys. D**3**, 401 (1986).

[13] L. A. Morgan, P. G. Burke, and C. J. Gillan, J. Phys. B**23**, 99 (1990).

[14] I. I. Fabrikant, S. A. Kalin, and A. K. Kazansky, J. Chem. Phys. **95**, 4966 (1991).

[15] P. L. Gertitschke and W. Domcke, Z. Phys. D**31**, 171 (1994).

[16] M. A. Morrison, Adv. At. Mol. Phys. **24**, 51 (1988).

[17] W. Domcke, Phys. Rep. **208**, 97 (1991).

[18] J. Horáček and W. Domcke, Phys. Rev. A**53**, 2262 (1996).

[19] J. Horáček, W. Domcke, and H. Nakamura, Z. Phys. D**42**, 181 (1997).

[20] J. Horáček, M. Čížek, and W. Domcke, Theor. Chem. Acc. **100**, 31 (1998).

[21] J. F. Ogilvie, W. R. Rodwell, and R. H. Tipping, J. Chem. Phys. **73**, 5221 (1980).

[22] N. T. Padial and D. W. Norcross, Phys. Rev. A**29**, 1590 (1984).

[23] S. V. O'Neil, P. Rosmus, D. W. Norcross, and H.-J. Werner, J. Chem. Phys. **85**, 7232 (1986).

[24] P. Åstrand and G. Karlström, Chem. Phys. Lett. **175**, 624 (1990).

[25] J. P. Gauyacq, J. Phys. B**15**, 2721 (1982).

[26] M. Čížek, J. Horáček, and W. Domcke, J. Phys. B**31**, 2571 (1998).

[27] R. J. Bieniek, Phys. Rev. A**18**, 392 (1978).

[28] H.-D. Meyer, J. Horáček, and L. S. Cederbaum, Phys. Rev. A**43**, 3587 (1991).

[29] H. J. Werner and P. Rosmus, J. Chem. Phys. **73**, 2319 (1980).

[30] M. A. Huels, J. A. Fedchak, R. L. Champion, L. D. Doverspike, J. P. Gauyacq, and D. Teillet-Billy, Phys. Rev. A**49**, 255 (1994).

[31] C. J. Howard, F. C. Fehsenfeld, and M. McFarland, J. Chem. Phys. **60**, 5068 (1974).

[32] V. Pless, B. M. Nestmann, and S. D. Peyerimhoff, J. Phys. B**25**, 4649 (1992).

[33] M. Allan and S. F. Wong, J. Chem. Phys. **74**, 1687 (1981).

[34] G. Knoth, M. Gote, M. Rädle, F. Leber, K. Jung, and H. Ehrhardt, J. Phys. B**22**, 2797 (1989).

[35] G. Knoth, M. Rädle, M. Gote, H. Ehrhardt, and K. Jung, J. Phys. B**22**, 299 (1989).

[36] M. Rädle, G. Knoth, K. Jung, and H. Ehrhardt, J. Phys. B**22**, 1455 (1989).

[37] M. Movre and W. Meyer, J. Chem. Phys. **106**, 7139 (1997).

FIGURES

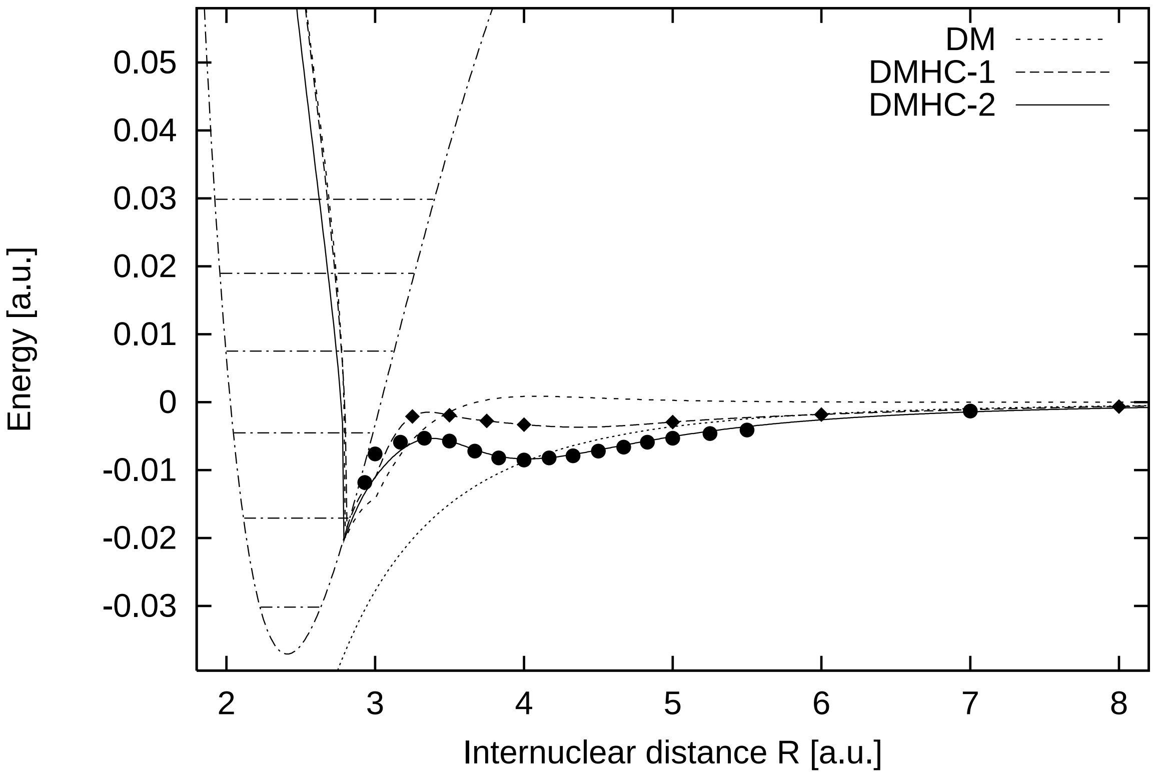

FIG. 1. Potential-energy function $V_0(R)$ of the $X^1\Sigma$ state of HCl (dashed-dotted curve, bound states indicated), potential-energy function $V_1(R)$ of the $^2\Sigma$ state of HCl$^-$ in the DM (short dashes), DMHC-1 (long dashes) and DMHC-2 (full curve) models. The dotted line shows the long-range polarization potential. Ab initio data of Åstrand and Karlström [24] and O'Neil et al. [23] are indicated by full circles and diamonds, respectively.

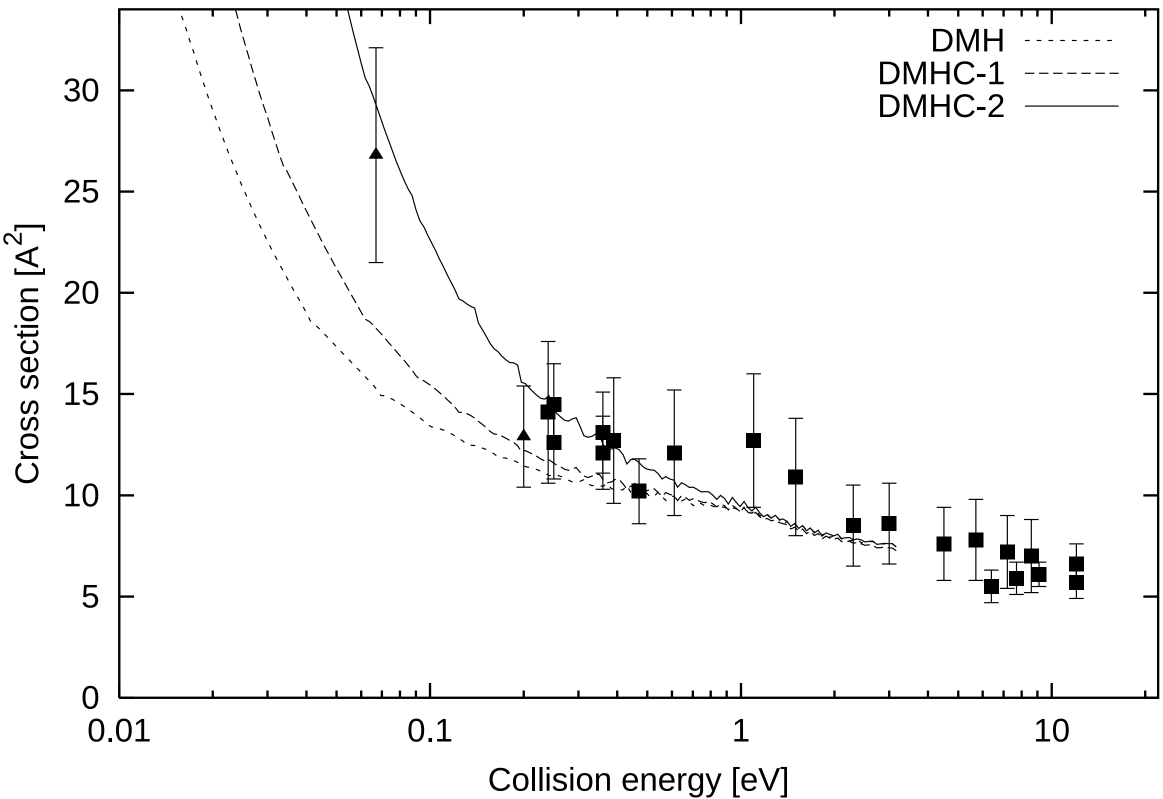

FIG. 2. The total associative detachment cross section obtained with the DMH (short dashes), DMHC-1 (long dashes) and DMHC-2 models (full curve), respectively. Experimental data (squares) and data derived from experimental rates (triangles) are taken from Huels et al. [30].

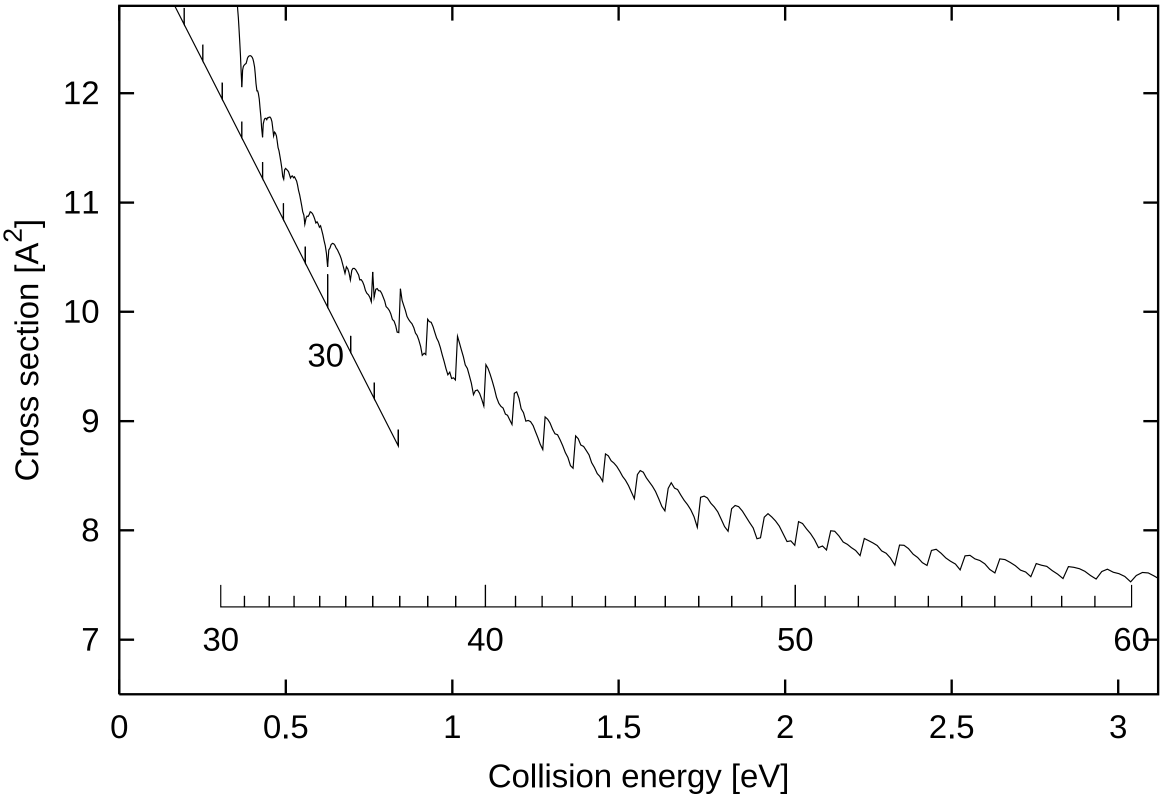

FIG. 3. Details of the threshold structures in the associative detachment cross section obtained with the DMHC-2 model. Thresholds for the production of HCl in ground and first excited vibrational states are indicated. The numbers give the angular momentum of the molecule in the final state.

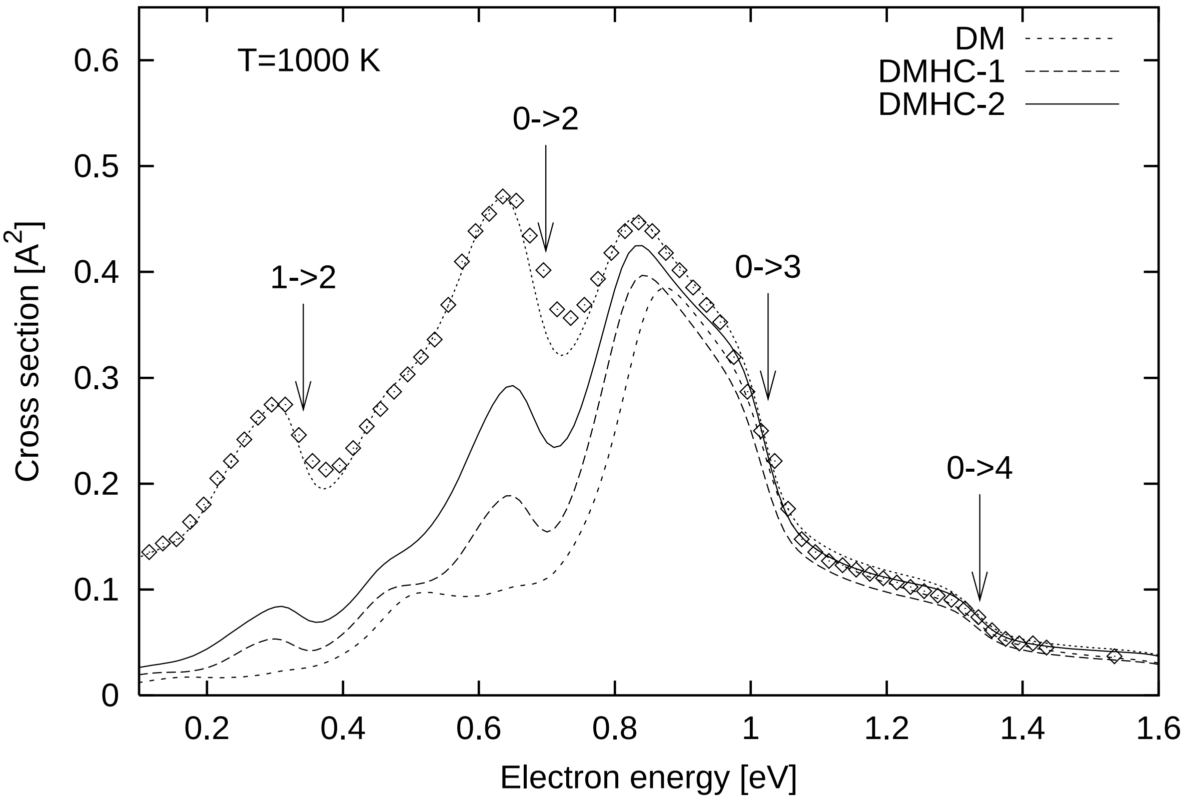

FIG. 4. Cross section for dissociative attachment in HCl gas with temperature $T = 1000$K. Diamonds are experimental values shifted by +35meV (see text) and normalized to the maximum of the dotted curve. The dots are the results of the DMHC-2 model for a temperature of 1230 K. Theoretical results are convoluted with Gaussian distribution of width 50meV FWHM. The full, long-dashed, and short-dashed curves are the results of the DMHC-2, DMHC-1 and DM models at $T = 1000$K, respectively. Vibrational excitation thresholds are indicated by arrows.

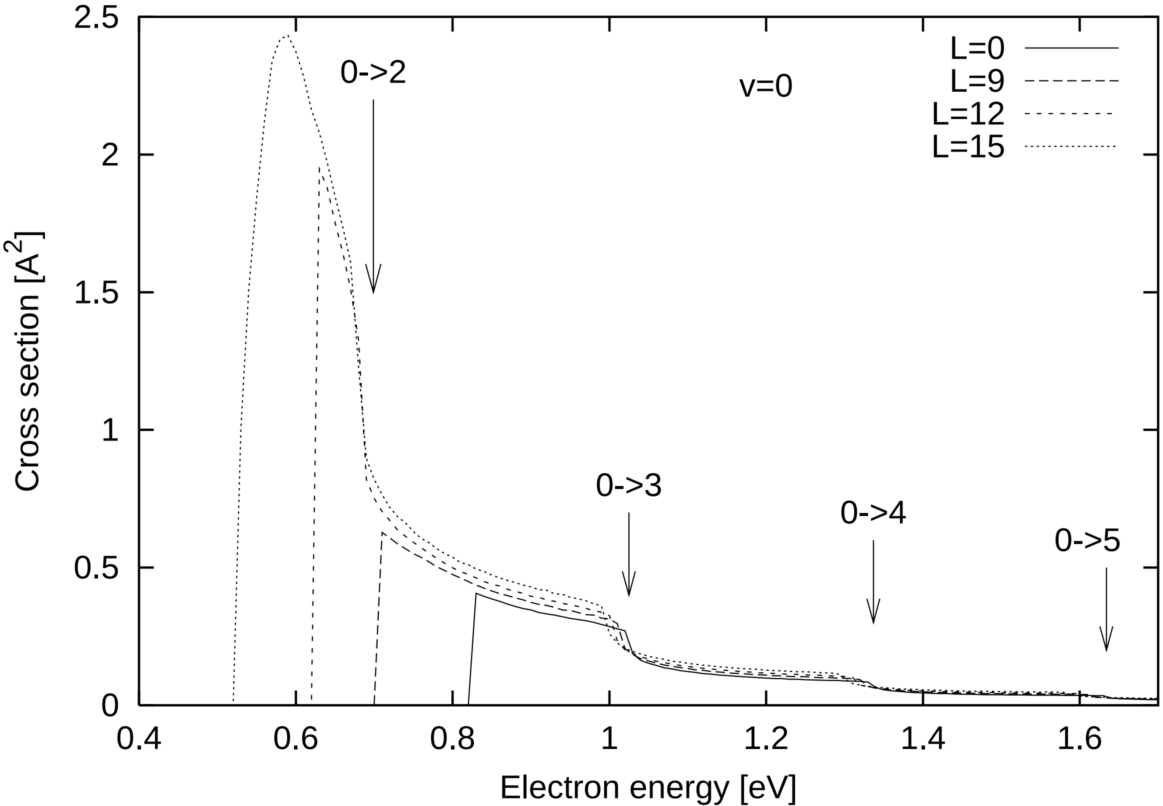

FIG. 5. Dependence of the $\nu = 0$ dissociative attachment cross section on the initial rotational state of the HCl molecule for the DMHC-2 model. Thresholds for vibrational excitation processes are indicated by arrows.

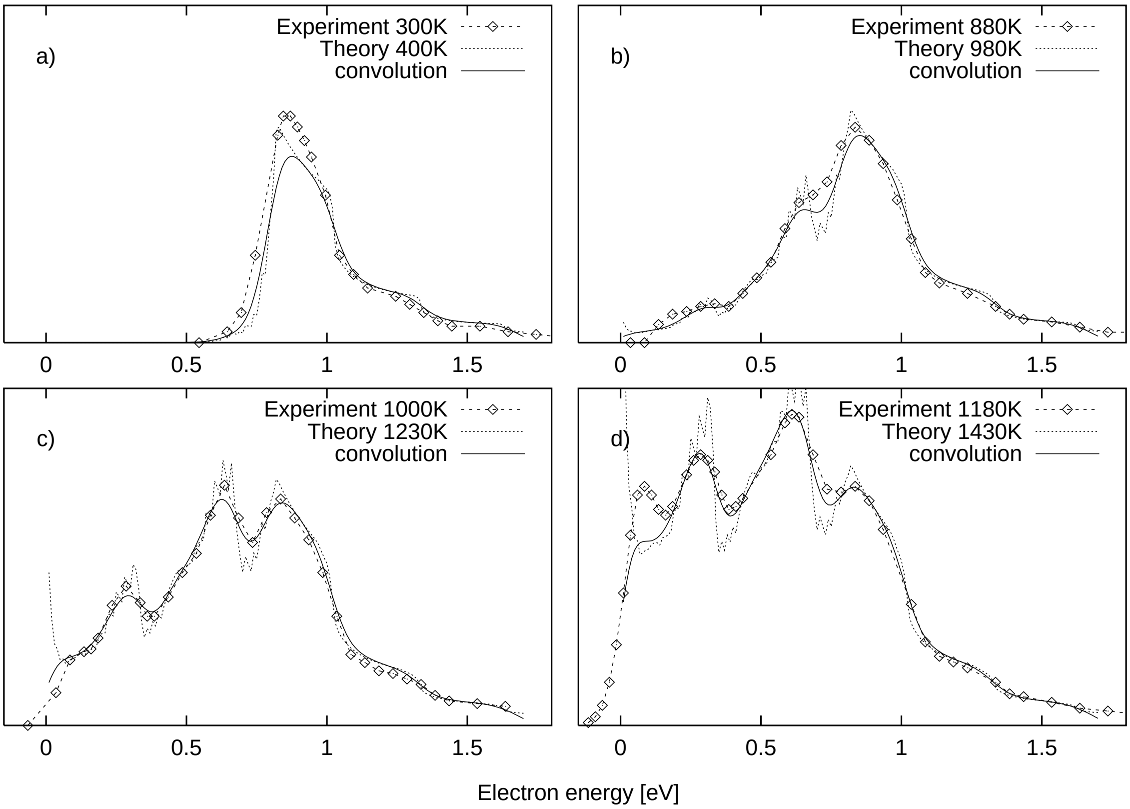

FIG. 6. Comparison of the theoretical dissociative attachment cross section with the experimental data of Allan and Wong [33]. The theoretical results are convoluted with a Gaussian of 100meV FWHM. The experimental data are shifted to higher energies by 35meV. The temperature yielding the closest agreement with experiment is chosen in the calculation (DMHC-2 model).

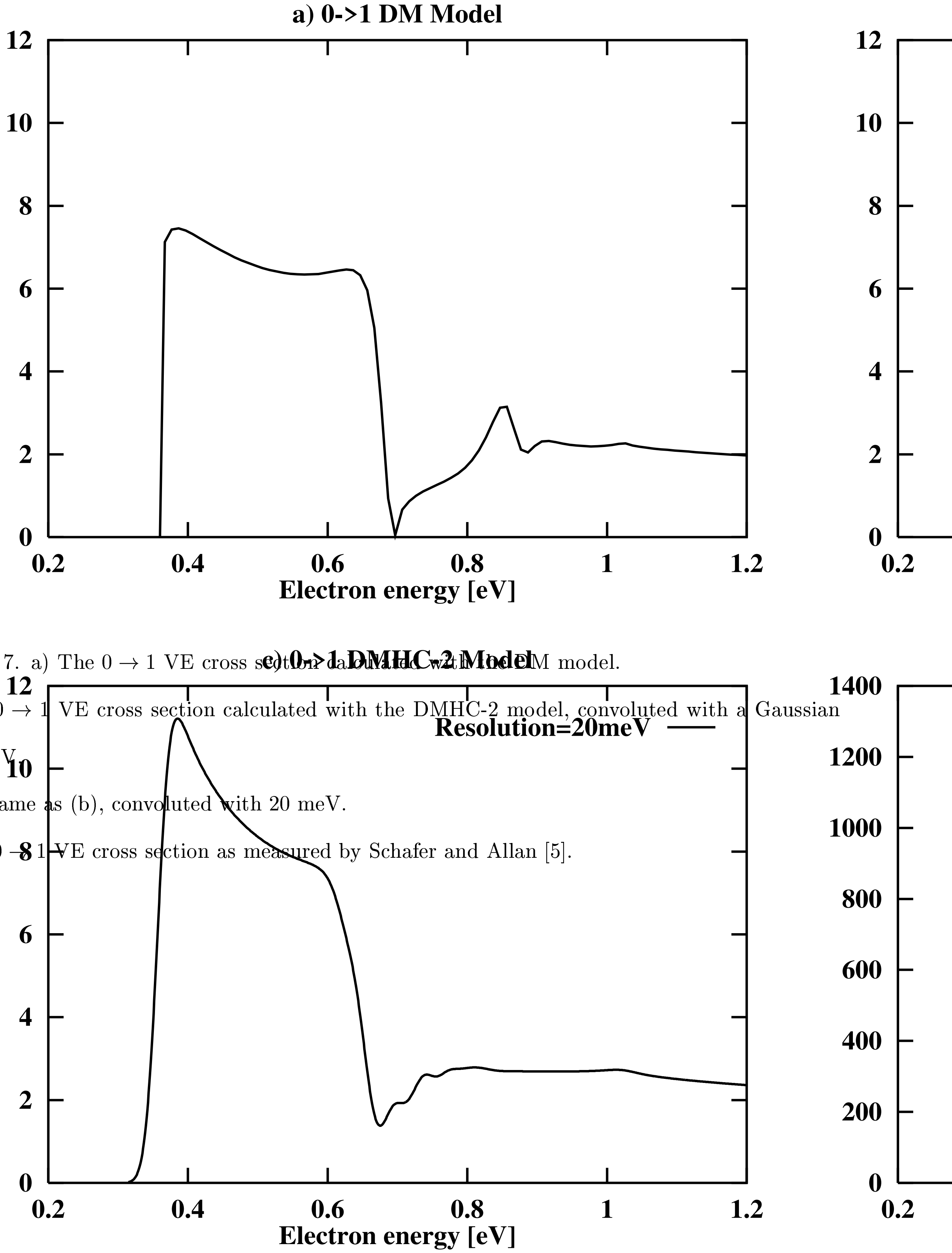

FIG. 7. a) The 0 → 1 VE cross section calculated with the DM model.

b) The 0 → 1 VE cross section calculated with the DMHC-2 model, convoluted with a Gaussian of 10 meV.

c) The same as (b), convoluted with 20 meV.

d) The 0 → 1 VE cross section as measured by Schafer and Allan [5].

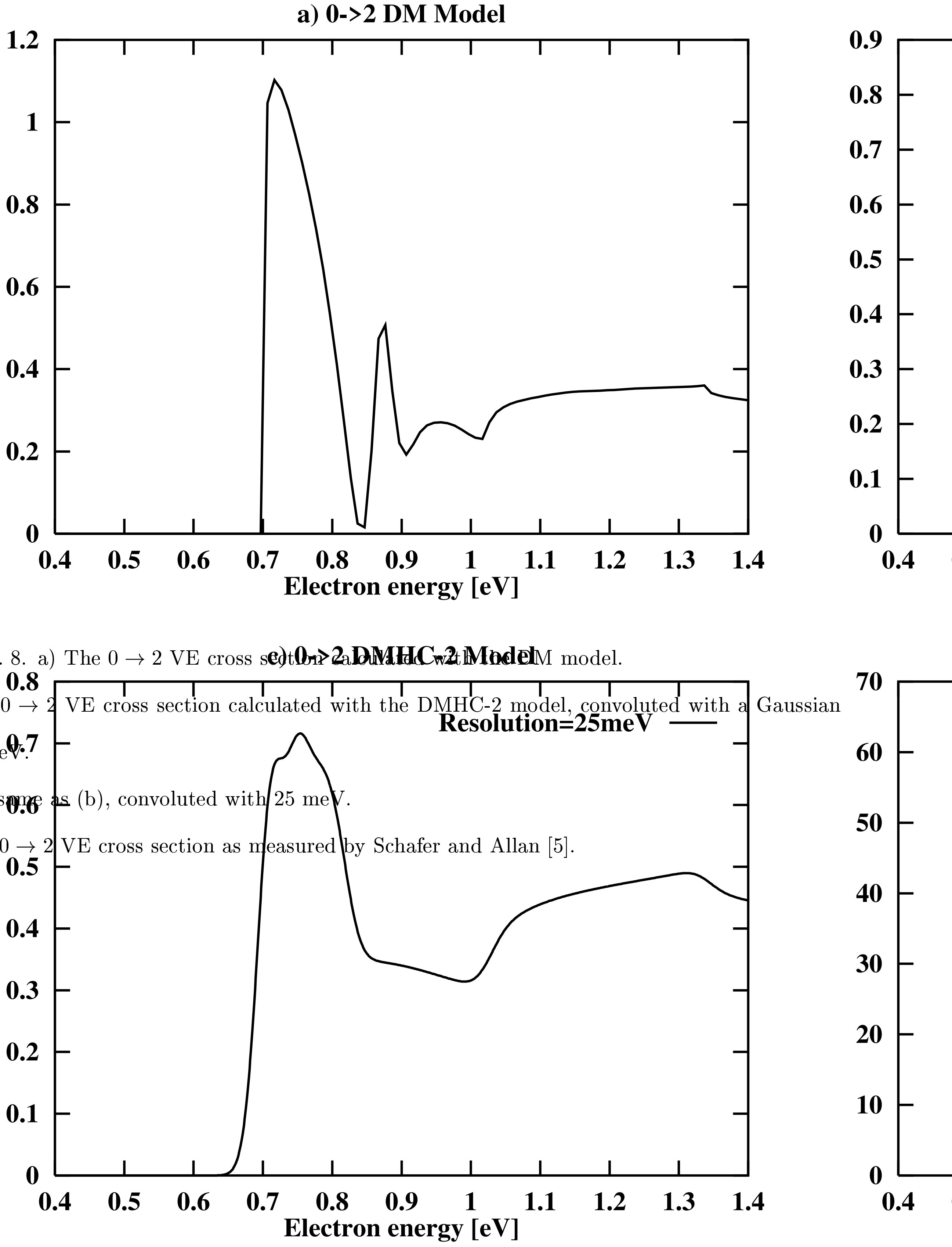

FIG. 8. a) The 0 → 2 VE cross section calculated with the DM model.

b) The 0 → 2 VE cross section calculated with the DMHC-2 model, convoluted with a Gaussian of 15 meV.

c) The same as (b), convoluted with 25 meV.

d) The 0 → 2 VE cross section as measured by Schafer and Allan [5].

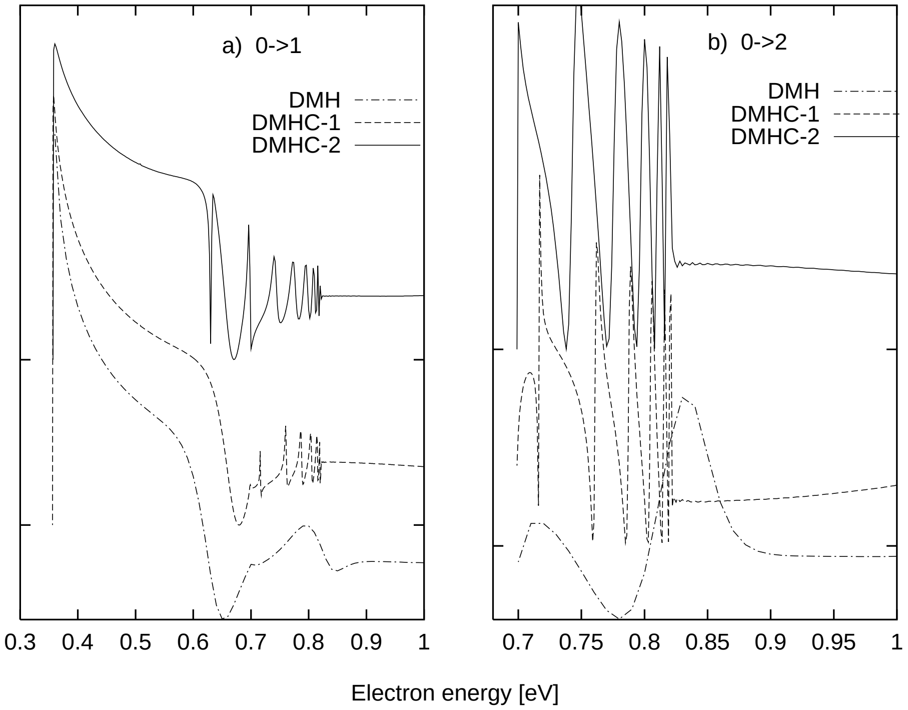

FIG. 9. 0 → 1 and 0 → 2 vibrational excitation cross sections near threshold. The results of the DMH, DMHC-1 and DMHC-2 models are shown, reflecting the influence of the long-range part of the HCl^- potential function.

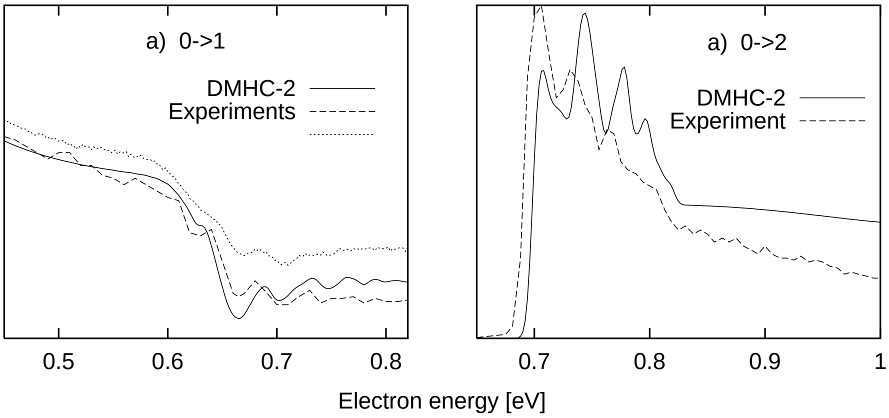

FIG. 10. Comparison of the calculated near-threshold 0 → 1 and 0 → 2 vibrational excitation cross sections (DMHC-2 model) with the high-resolution measurements of Schafer and Allan [5] (dots) and Cvejanović [4] (dashes). The theoretical data are thermally averaged (T=300K) and convoluted with a Gaussian of 30meV FWHM.

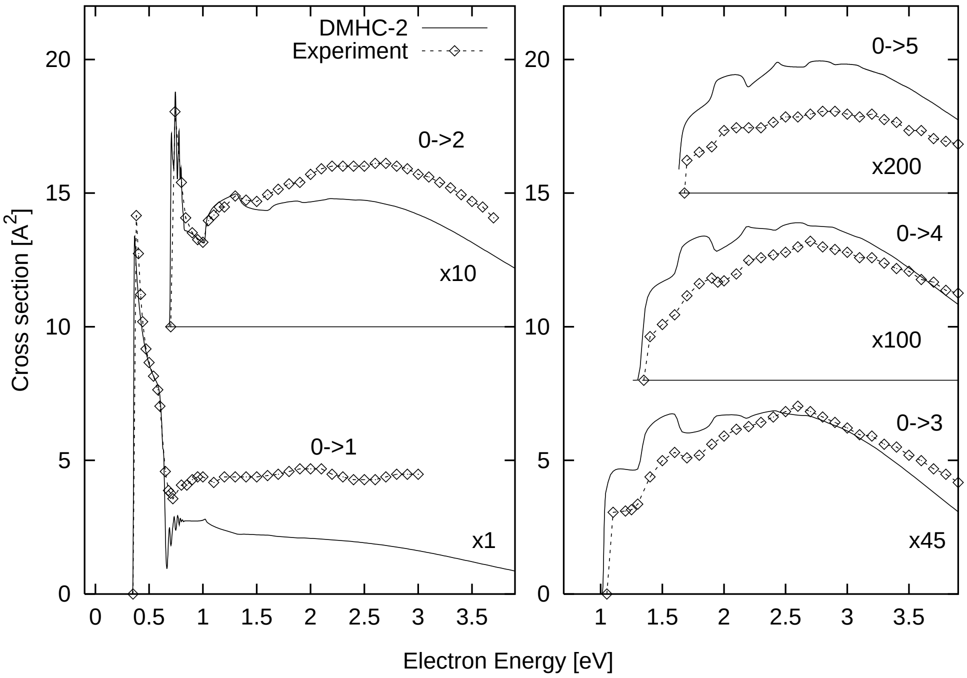

FIG. 11. Comparison of the calculated vibrational excitation cross sections with the experimental data of Schafer and Allan [5]. The data are scaled (see labels). The overall normalization of the experimental data is chosen to give agreement with theory for the $0 \to 2$ cross section near 1eV.